Targeting annexin A7 by a small molecule suppressed the activity of phosphatidylcholine-specific phospholipase C in vascular endothelial cells and inhibited atherosclerosis in apolipoprotein E $^{-/-}$ mice

H Li[1], S Huang[1], S Wang[2], J Zhao[1], L Su[1], B Zhao*[,2], Y Zhang[3], S Zhang[1] and J Miao*[,1,3]

Phosphatidylcholine-specific phospholipase C (PC-PLC) is a key factor in apoptosis and autophagy of vascular endothelial cells (VECs), and involved in atherosclerosis in apolipoprotein E $^{-/-}$ (apoE $^{-/-}$) mice. But the endogenous regulators of PC-PLC are not known. We recently found a small chemical molecule (6-amino-2, 3-dihydro-3-hydroxymethyl-1, 4-benzoxazine, ABO) that could inhibit oxidized low-density lipoprotein (oxLDL)-induced apoptosis and promote autophagy in VECs, and further identified ABO as an inhibitor of annexin A7 (ANXA7) GTPase. Based on these findings, we hypothesize that ANXA7 is an endogenous regulator of PC-PLC, and targeting ANXA7 by ABO may inhibit atherosclerosis in apoE $^{-/-}$ mice. In this study, we tested our hypothesis. The results showed that ABO suppressed oxLDL-induced increase of PC-PLC level and activity and promoted the co-localization of ANXA7 and PC-PLC in VECs. The experiments of ANXA7 knockdown and overexpression demonstrated that the action of ABO was ANXA7-dependent in cultured VECs. To investigate the relation of ANXA7 with PC-PLC in atherosclerosis, apoE $^{-/-}$ mice fed with a western diet were treated with 50 or 100 mg/kg/day ABO. The results showed that ABO decreased PC-PLC levels in the mouse aortic endothelium and PC-PLC activity in serum, and enhanced the protein levels of ANXA7 in the mouse aortic endothelium. Furthermore, both dosages of ABO significantly enhanced autophagy and reduced apoptosis in the mouse aortic endothelium. As a result, ABO significantly reduced atherosclerotic plaque area and effectively preserved a stable plaques phenotype, including reduced lipid deposition and pro-inflammatory macrophages, increased anti-inflammatory macrophages, collagen content and smooth muscle cells, and less cell death in the plaques. In conclusion, ANXA7 was an endogenous regulator of PC-PLC, and targeting ANXA7 by ABO inhibited atherosclerosis in apoE $^{-/-}$ mice.

Apoptosis and autophagy are two evolutionarily conserved processes that maintain homeostasis during stress.[1] Although the two pathways utilize fundamentally distinct machinery, apoptosis and autophagy are highly interconnected and share many key regulators.[2] Phosphatidylcholine-specific phospholipase C (PC-PLC), an important member of the phospholipase family, has been implicated in several cellular signaling pathways.[3] Our laboratory is dedicated to researching the role of PC-PLC in the regulation of vascular endothelial cell (VEC) apoptosis.[4] We found that PC-PLC was involved in human umbilical vein endothelial cell (HUVEC) apoptosis that was induced by deprivation of fibroblast growth factor and serum, and also by rattlesnake venom.[5] In addition, our previous studies indicated the roles of PC-PLC in VEC

apoptosis and senescence, and found that inhibition of PC-PLC by its inhibitor D609 suppressed VEC apoptosis and senescence.[4] Furthermore, we found that Cd^{2+} at low concentrations could promote VEC autophagy and inhibit VEC apoptosis by depressing PC-PLC activity,[6] which suggests that PC-PLC may function as a pro-apoptosis factor. Based on the relationship of apoptosis and autophagy, recently, we detected decreased PC-PLC activity during HUVEC autophagy induced by Cd^{2+} and sphingosylphosphorylcholine.[6,7] Collectively, PC-PLC is a key factor in apoptosis and autophagy of VECs.

In addition, our recent *in vivo* study demonstrated that PC-PLC was involved in atherosclerosis in apolipoprotein E $^{-/-}$ (apoE $^{-/-}$) mice.[8] PC-PLC is upregulated in the endothelial

[1]Shandong Provincial Key Laboratory of Animal Cells and Developmental Biology, Institute of Developmental Biology, School of Life Science, Shandong University, Jinan, China; [2]Institute of Organic Chemistry, School of Chemistry and Chemical Engineering, Shandong University, Jinan, China and [3]The Key Laboratory of Cardiovascular Remodeling and Function Research, Chinese Ministry of Education and Chinese Ministry of Health, Shandong University Qilu Hospital, Jinan, China
*Corresponding authors: J Miao or B Zhao, Shandong Provincial Key Laboratory of Animal Cells and Developmental Biology, Institute of Developmental Biology, School of Life Science, Shandong University, Jinan 250100, China. Tel: +86 531 88364929; Fax: +86 531 88565610; E-mails: miaojy@sdu.edu.cn or bxzhao@sdu.edu.cn

cell layer in the atherosclerotic lesions. Pharmacological blockade of PC-PLC by D609 inhibited the progression of pre-existing atherosclerotic lesions in apoE $^{-/-}$ mice and changed the lesion composition into a more stable phenotype. These data suggest that PC-PLC is involved in the progression and destabilization of established atheroma. Our results also showed that the atherogenic effect of PC-PLC was acting through the regulation of endothelial expression of LOX-1, adhesion molecules VCAM-1 and ICAM-1, and chemokine MCP-1. Taken together, PC-PLC contributed to the progression of atherosclerosis. PC-PLC might serve as a marker in the diagnosis of atherosclerosis in the future and provide a new target for atherosclerosis therapy.

Because the changes of PC-PLC activity have been detected in apoptosis, autophagy and inflammation, endogenous regulators of PC-PLC activity may exist, but, which are not clear so far. Furthermore, it is regretful that a major gap in our knowledge of this important enzyme is linked to the fact that the mammalian PC-PLC has not been cloned and its sequence is unknown.[9] Genetic deletion or overexpression of PC-PLC is unavailable, and exploiting its inhibitor D609 (tricyclodecan-9-yl-xanthogenate) and performing the activity assay have been the strategies for the study of the functions of PC-PLC in mammalian cells.[8]

We recently found a small chemical molecule (6-amino-2, 3-dihydro-3-hydroxymethyl-1, 4-benzoxazine, ABO, Supplementary Figure 1) that could inhibit oxidized low-density lipoprotein (oxLDL)-induced apoptosis[10] and promote autophagy in VECs via annexin A7 (ANXA7).[11] ANXA7, a member of the annexin family of calcium-dependent phospholipid binding proteins, codes for Ca^{2+}- dependent GTPase. In the last decade, we, and others, have shown that ANXA7 has several different roles in autophagy, exocytosis, carcinogenesis and tumor suppression.[11–15] However, whether ANXA7 participates in the promotion or inhibition of atherosclerosis progression is unclear. Furthermore, knockout mouse is not an ideal model for ANXA7 research in disease, because homozygous ANXA7 ($^{-/-}$) mutation is lethal by E10,[16] and ANXA7($^{+/-}$) mutation also has several unwished phenotypes, such as induce β-cell hypertrophy, islet hyperplasia, an alteration in the Ca^{2+} dependence of glucose-induced insulin secretion, and aberrant regulation of islet gene expression by the fed/fasted state.[17] Fortunately, in a recent study, we found that ABO could directly bind to ANXA7 and inhibit phosphorylation of ANXA7,[18] which had a significant inhibitory effect on its GTPase activity.[19] Our findings suggest that as a small molecule modulator of ANXA7 function, ABO is a powerful tool to study the complex cellular functions of ANXA7.

As described above, we found that HUVEC apoptosis induced by oxLDL[10] accompanied by PC-PLC activation,[8] whereas ABO could directly target ANXA7,[18] induce autophagy in cultured VECs[11] and inhibit VEC apoptosis induced by oxLDL,[10] suggesting that there may be an interaction between ANXA7 and PC-PLC in VECs. Moreover, treatment of isolated lung lamellar bodies with PC-PLC enhances the ANXA7 fusion activity via increasing diacylglycerol level.[20]
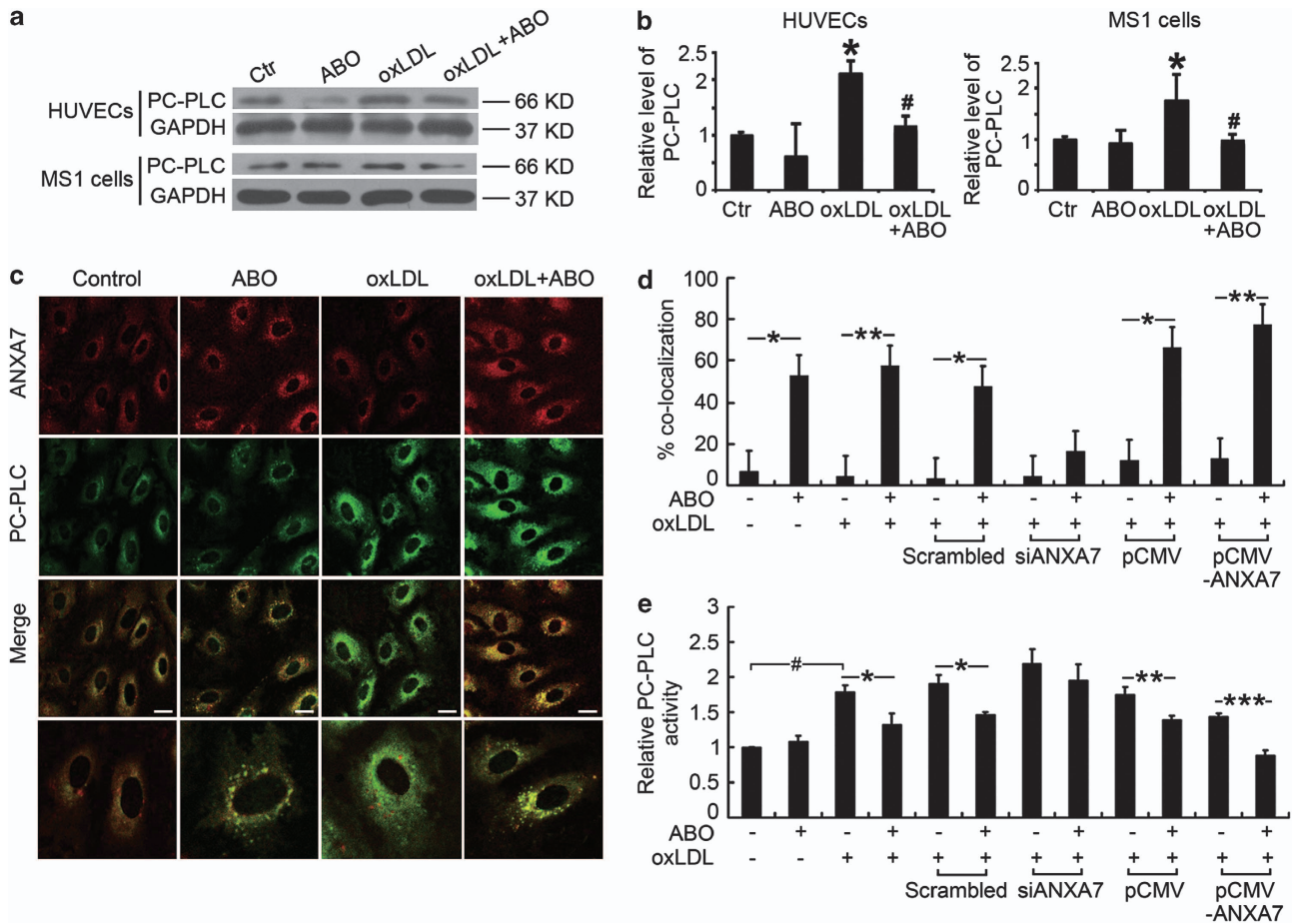
Based on these findings, we hypothesize that ANXA7 is an endogenous regulator of PC-PLC, and targeting ANXA7 by ABO may inhibit atherosclerosis in apoE $^{-/-}$ mice. In this study, we tested our hypothesis.

Results

ABO suppressed oxLDL-induced PC-PLC level in cultured ECs. As PC-PLC involved in oxLDL-induced HUVEC apoptosis, which was significantly inhibited by ABO, we first tested the effect of ABO on the protein level of PC-PLC in cultured HUVECs and MS1 cells. In line with our previous report, western blot analyses showed that oxLDL increased PC-PLC level. However, the high levels of PC-PLC induced by oxLDL treatment were significantly inhibited by ABO both in cultured HUVECs and MS1 cells (Figures 1a and b).

ABO suppressed oxLDL-induced PC-PLC activity in an ANXA7-dependent manner in HUVECs. Because ABO increased ANXA7 level and reduced PC-PLC level, we wondered whether ANXA7 participated in the ABO-mediated PC-PLC inhibition in HUVECs. We used knockdown and overexpression of ANXA7, and confirmed the protein expression in HUVECs (Supplementary Figure S2). Consistent with previous results, ABO specifically increased ANXA7 level and oxLDL increased PC-PLC activity (Supplementary Figure S2 and Figure 1e). In addition, ABO could significantly increase the level of ANXA7 with oxLDL treatment and suppress oxLDL-induced PC-PLC activity in HUVECs, whereas silencing ANXA7 reversed the effect of ABO treatment as compared with scrambled siRNA. In addition, ANXA7 overexpression and ABO combined could strongly inhibit PC-PLC activity, but ANXA7 overexpression alone had no benefit on this action, which suggested that ABO may be indispensable in PC-PLC inhibition via ANXA7. Our previous findings advanced our understanding of the dual role of ABO in elevating the protein level and triggering ANXA7 subcellular redistribution, such as facilitating the co-localization of ANXA7 with microtubule-associated protein 1 light chain 3 (LC3) under normal condition.[11] These data reminded us that ABO might also trigger the subcellular redistribution of ANXA7 and PC-PLC, and subsequently inhibit the activity of PC-PLC induced by oxLDL. To test this hypothesis, we performed double-immunofluorescence staining of ANXA7 and PC-PLC under indicated treatment (Figures 1c and d). The micrographs demonstrated that the punctate pattern of PC-PLC induced by ABO was impaired in ANXA7-deficient cells. In addition, combined ANXA7 over-expression and ABO stimulus promoted PC-PLC patch and the co-localization of ANXA7 and PC-PLC, whereas over-expression alone failed to demonstrate any significant benefit of this action (Supplementary Figure S3). Moreover, opposite trends in PC-PLC activity and quantification of the co-localization with ANXA7 were shown in Figures 1d and e. Taken together, these results confirmed the hypothesis that ABO suppressed oxLDL-induced PC-PLC activity via the co-localization of ANXA7 and PC-PLC in an ANXA7-dependent manner.

PC-PLC level in aortic roots and serum activity were decreased by ABO. Our recent *in vivo* study demonstrated that PC-PLC contributed to the progression of atherosclerosis by promoting the production of pro-inflammatory cytokines.[8] Therefore, we tested the effect of ABO on PC-PLC level and activity *in vivo*. Double-immunofluorescence staining showed

Figure 1 ABO treatment inhibited the increased level and activity of PC-PLC induced by oxLDL in endothelial cells via promoting co-localization of ANXA7 and PC-PLC in an ANXA7-dependent manner. (**a**) Effects of ABO on the protein levels of PC-PLC in HUVECs and MS1 cells under oxLDL treatment detected by western blot analysis. ABO (50 μM) and oxLDL (50 μg/ml for HUVECs and 100 μg/ml for MS1 cells) were used. (**b**) Quantification of PC-PLC protein levels shown in A. Protein levels were normalized to GAPDH. Values are mean $\pm$ S.E.M. *$P < 0.05$, versus control, #$P < 0.05$, versus oxLDL, $n = 3$. (**c**) Double immunohistochemical staining showed that ANXA7 (red) and PC-PLC (green) exhibited agglomeration and co-localization after ABO treatment in HUVECs upon oxLDL stimulus. Overlays of the red and green signal with a yellow color indicated co-localization. Scale bars, 16 μm. (**d** and **e**) Overexpression (pCMV-ANXA7) and knockdown (siANXA7) of ANXA7 were performed. (**d**) Analysis of co-localization between ANXA7 and PC-PLC in HUVECs. Co-localization in confocal microscopy is defined by the presence of three or more ANXA7 and PC-PLC residing at the same physical location in a specimen. The bar chart shows quantification of co-localization of ANXA7 and PC-PLC. Data are mean $\pm$ S.E.M. *$P < 0.05$, **$P < 0.01$; $n = 3$. (**e**) Quantification of PC-PLC activity. Data are mean $\pm$ S.E.M. *$P < 0.05$, **$P < 0.01$, ***$P < 0.001$, #$P < 0.05$, $n = 3$

that low-dosage ABO slightly and nonsignificantly decreased the protein level of PC-PLC, but high-dosage ABO significantly reduced the level as compared with controls (Figures 2a and b). As well, the mean serum PC-PLC activity was lower with ABO treatment than controls (Figure 2c). Collectively, ABO could suppress PC-PLC level and activity *in vivo*.

ABO elevated ANXA7 level in the mouse aortic endothelium. To further elucidate the mechanism by which ABO inhibits PC-PLC *in vivo*, we assessed the level of ANXA7 in aortic ECs by immunofluorescence analysis. The aortic roots of ABO-treated groups showed significantly increased staining for ANXA7 as compared with controls (Figure 3), suggesting that ABO performed PC-PLC inhibition via ANXA7 *in vivo*.

ABO stimulated autophagy in VECs under proatherogenic conditions *in vitro* and *in vivo*. To further elucidate the

induction of autophagy by ABO under proatherogenic conditions, we first performed *in vitro* experiments in HUVECs and MS1 cells with oxLDL treatment. Western blot analyses showed that ABO treatment significantly elevated the level of LC3-II and the ratio of LC3-II/LC3-I both in HUVECs and MS1 cells (Figures 4a and b). Next, to test whether ABO could induce autophagy *in vivo*, we assessed the level of autophagy in the VEC layer of advanced atherosclerotic lesions from the aortic roots of apoE$^{-/-}$ mice by transmission electron microscopy (TEM) and immunofluorescence analysis. TEM revealed autophagy activation in the aortic endothelium of ABO-treated mice, as shown by an increase in autophagosomes (Figures 4c and d). Immature autophagic vacuoles characterized by an electron density equivalent to the cytoplasm coexisted with late vesicles characterized by increased electron density, in which catabolic processes had already started. In addition, the increase of LC3 puncta could reflect induction of autophagy.[21] We then performed en face immufluorescence
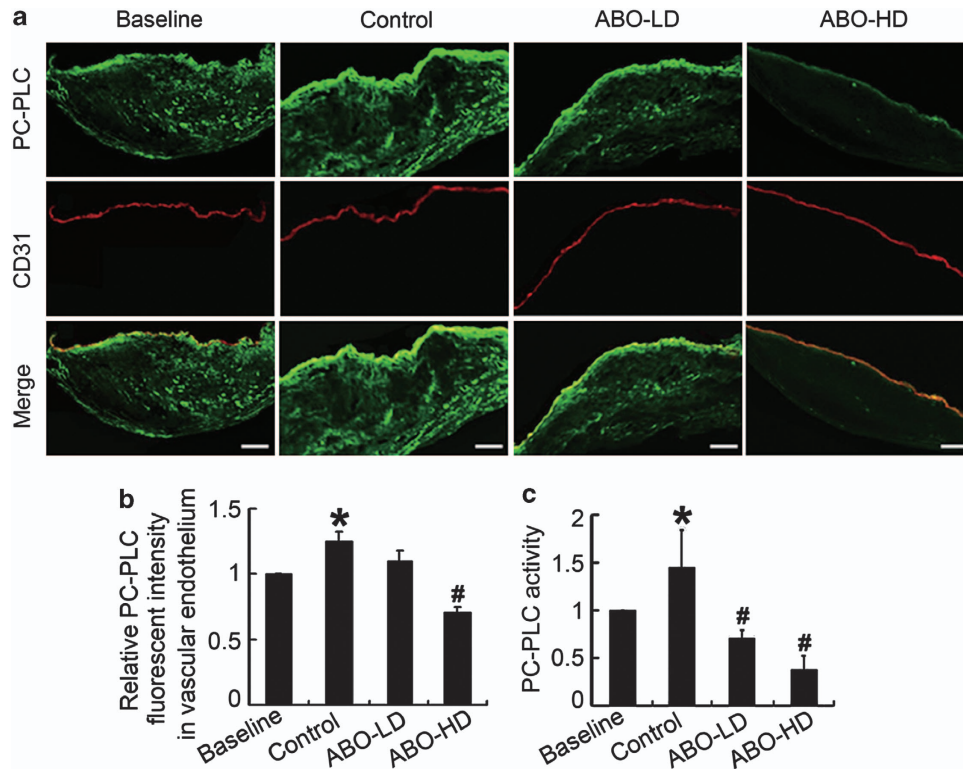
Figure 2 ABO treatment inhibited the increased level and activity of PC-PLC in apoE$^{-/-}$ mice. (**a**) Double-stained images of co-localization (yellow) of PC-PLC and CD31-positive VECs. Scale bars, 60 μm. (**b**) Quantification of PC-PLC level in endothelium of baseline, control and ABO-treated groups. Data are mean ± S.E.M. *$P < 0.05$ versus baseline, #$P < 0.05$ versus control, $n = 6$. (**c**) Relative PC-PLC activity normalized to baseline activity (equal to 1). Data are mean ± S.E.M. *$P < 0.05$ versus baseline, #$P < 0.05$ versus control, $n = 6$
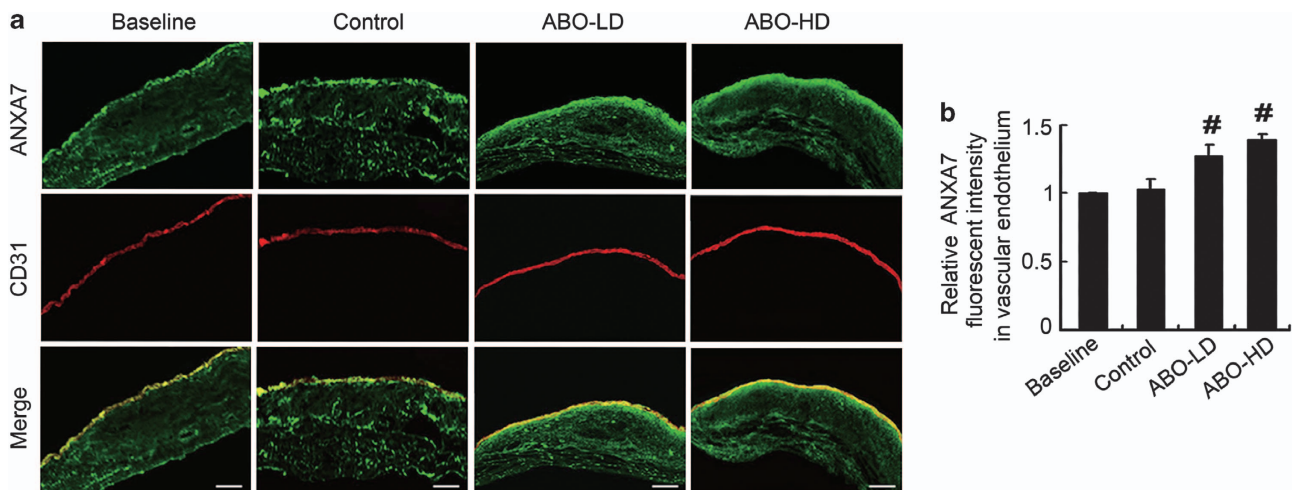
Figure 3 ABO increased ANXA7 level in the endothelium of apoE$^{-/-}$ mice. (**a**) Double-stained images of co-localization (yellow) of ANXA7 with CD31-positive VECs. Scale bars, 60 μm. (**b**) The relative fluorescent intensity of ANXA7 in the endothelium of apoE$^{-/-}$ mice. Data are mean ± S.E.M. #$P < 0.05$ versus control, $n = 6$

analysis of LC3 in the endothelium and quantified the average number of LC3 puncta per cell (Figures 4e and f, Supplementary Figure S4). The results showed that the number of LC3 puncta was significantly increased by ABO treatment, suggesting that ABO promoted autophagy in the endothelium. p62/SQSTM1, as an autophagy substrate, is known to accumulate with defective autophagic flux through lysosomes (i.e., by decreased p62 lysosomal degradation).[22–24] We further investigated the changes of p62 protein level in HUVECs and MS1 cells with treatment of oxLDL, ABO or both. ABO suppressed the oxLDL-increased protein level of p62 in HUVECs and MS1 cells (Figures 5a and b). Subsequently, we performed immunofluorescence analysis of p62 protein in the atherosclerotic lesion. The results showed that p62 protein level was also increased in endothelium of advanced atherosclerotic plaques, and
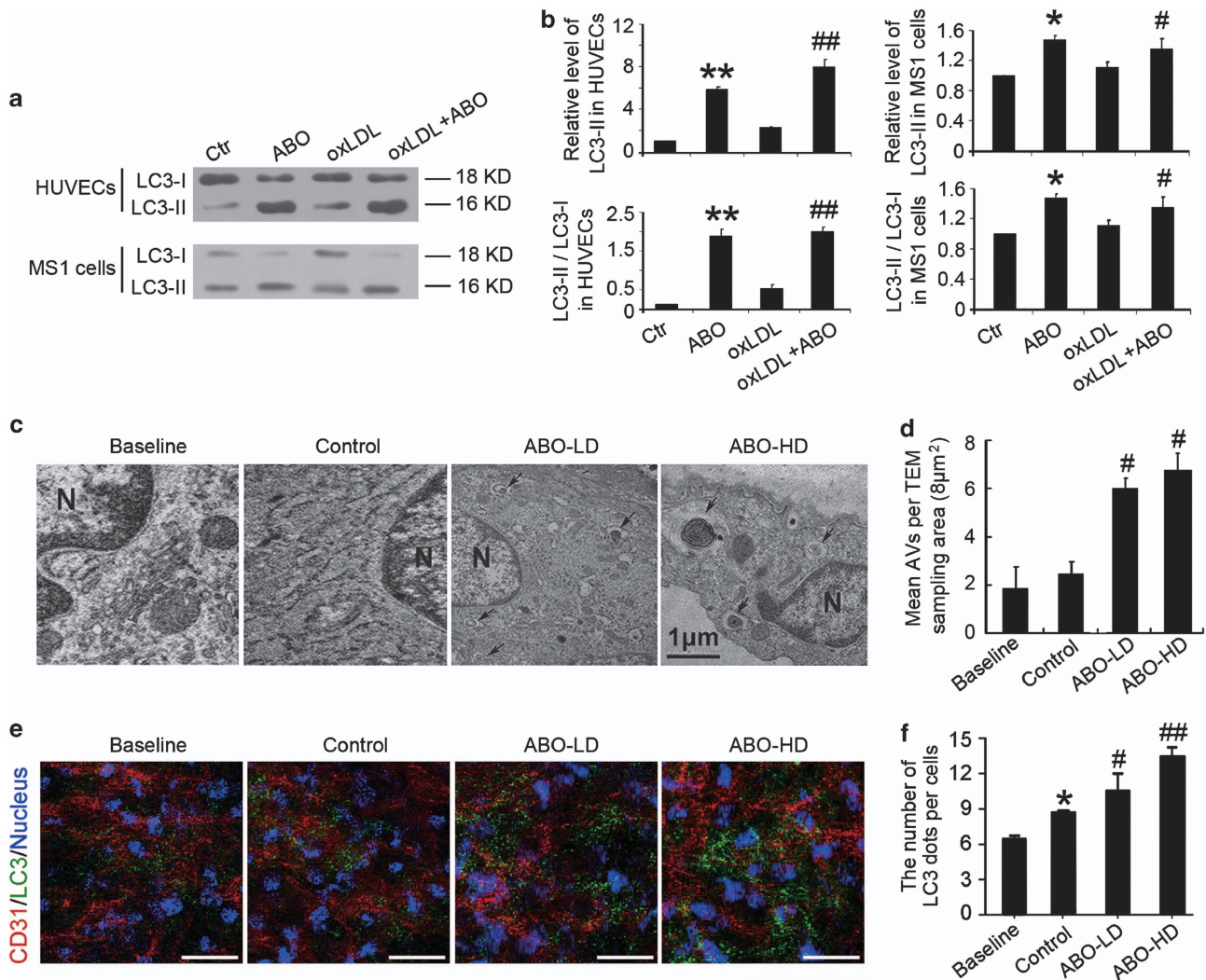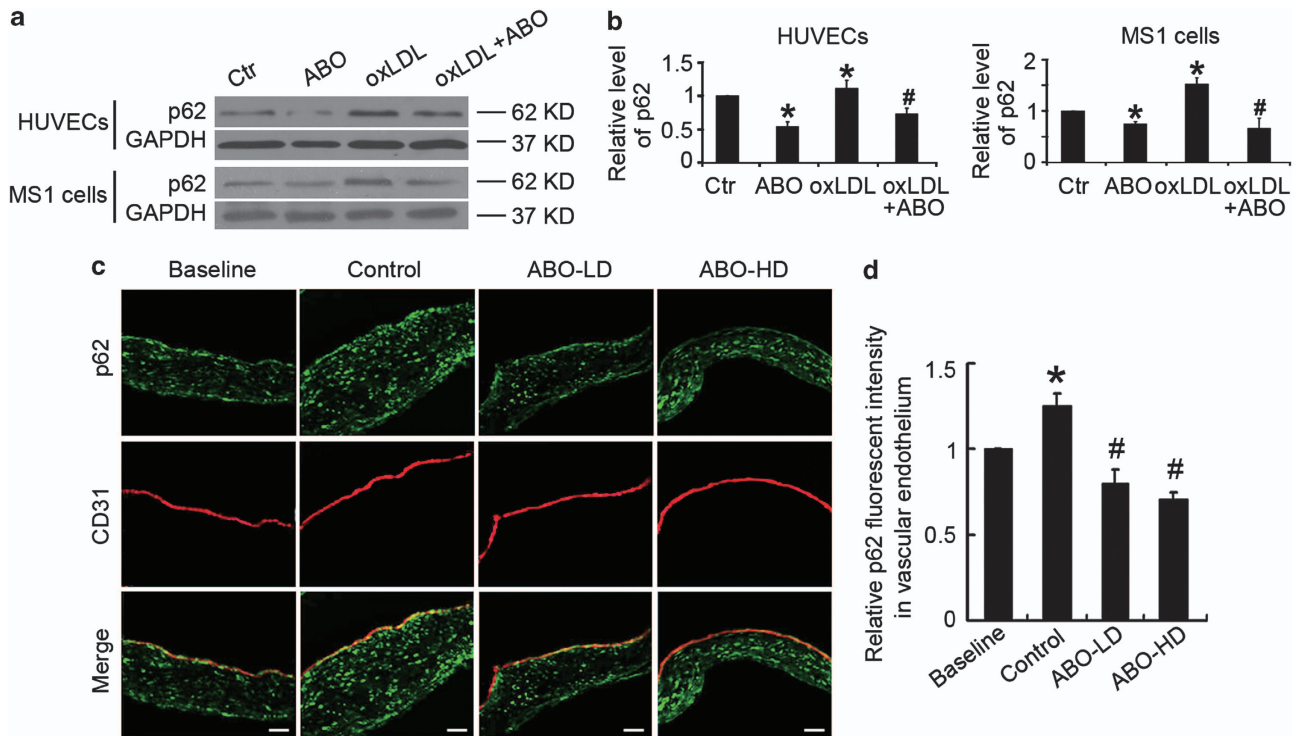
Figure 4 ABO induced autophagy in cultured endothelial cells under oxLDL treatment and in the endothelium of apoE$^{-/-}$ mice. (**a**) Effects of ABO on the protein level of LC3-II and LC3-I conversion in HUVECs and MS1 cells under oxLDL treatment detected by western blot analysis. ABO (50 μM) and oxLDL (50 μg/ml for HUVECs and 100 μg/ml for MS1 cells) were used. (**b**) Quantification of LC3-II protein levels and the ratio of LC3-II/LC3-I shown in **a**. Protein levels were normalized to GAPDH. Values are mean ± S.E.M. *P<0.05, **P<0.01 *versus* control, #P<0.05, ##P<0.01 *versus* oxLDL, n=3. (**c**) TEM of autophagosome formation in the endothelium of ABO-treated groups (N, nucleus; arrow, autophagosomes and autolysosomes). (**d**) Autophagic vesicles (AVs), including autophagosomes and autolysosomes, were counted from 8 μm^2 sampling regions per cell. Data are mean ± S.E.M. #P<0.05 *versus* control. (**e**) Dual immunofluorescence for CD31 and LC3 of en face aortic arch. Confocal images of en face aortic arch labeled with DAPI (blue), rat-anti-CD31 (red) and rabbit-anti-LC3 (green). Scale bars, 60 μm. (**f**) The bar chart separately showed quantification of LC3 dots per cell in the endothelium. Data are mean ± S.E.M. *P<0.05 *versus* baseline, #P<0.05, ##P<0.01 *versus* control, n=6

ABO inhibited this increase obviously (Figures 5c and d). All the data suggested that the autophagic flux in the atherosclerotic endothelium was increased by ABO treatment.

ABO suppressed cell death in the endothelium and in the plaques. Based on the cross talk between apoptosis and autophagy, we tested the effects of ABO on cell death of vascular cells within plaques, which have a key role in plaque instability.[25,26] We detected and quantified apoptosis and necrosis in the endothelium and in the plaques by terminal deoxynucleotidyl transferase-mediated dUTP nick-end labeling (TUNEL) staining and hematoxylin and eosin (H&E) staining, respectively. The results showed that the two types of cell death, albeit at low levels, at baseline and all levels, were

increased two- to three-fold in the control. However, both types of cell death were decreased in ABO-treated groups (Figure 6).

ABO restricted atherosclerosis development and stabilized established atherosclerotic lesion in apoE$^{-/-}$ mice. To further elucidate the involvement of ANXA7/PC-PLC in atherosclerosis, the effects of ABO on atherosclerosis development were investigated in apoE$^{-/-}$ mice. Oil-red O staining revealed significantly lower lipid-positive area with both high- and low-dosage ABO than control treatment in apoE$^{-/-}$ mice (Figure 7a). Morphometric assessment of plaque burden in the brachiocephalic artery and aortic root corroborated the anti-atherosclerotic effects of ABO on the mouse aorta (Figures 7b and c).

Figure 5 ABO decreased p62 level in cultured endothelial cells under oxLDL treatment and in the endothelium of apoE $^{-/-}$ mice. (**a**) Effects of ABO on the protein level of p62 in HUVECs and MS1 cells under oxLDL treatment detected by western blot analysis. ABO (50 μM) and oxLDL (50 μg/ml for HUVECs and 100 μg/ml for MS1 cells) were used. (**b**) Quantification of p62 protein levels shown in **a**. Protein levels were normalized to GAPDH. Values are mean ± S.E.M. *$P < 0.05$, *versus* control, #$P < 0.05$, *versus* oxLDL, $n = 3$. (**c**) Double-stained images of co-localization (yellow) of p62 with CD31-positive VECs. Scale bars, 60 μm. (**d**) The relative fluorescent intensity of p62 in the endothelium of apoE $^{-/-}$ mice. Data are mean ± S.E.M. *$P < 0.05$ *versus* baseline, #$P < 0.05$ *versus* control, $n = 6$

Next, we investigated the effect of ABO on the plaque phenotype. The results showed that ABO preserved a stable plaque phenotype, with increased collagen content and smooth muscle cells, and reduced lipid deposition. Moreover, ABO decreased pro-inflammatory macrophages known as M1 and increased anti-inflammatory macrophages known as M2[27] (Figures 7d and e).

The proteolytic enzymes matrix metalloproteinases (MMPs) are important in weakening the fibrous cap and promoting plaque rupture. Consistent with the previous results,[8] *in situ* zymography detected high activity of MMP-2/9 in atherosclerotic lesions with control treatment; the addition of ABO significantly reduced their activity (Figures 7d and e).

ABO did not affect body weight, organ coefficients and serum lipid levels of apoE $^{-/-}$ mice. Further, we performed toxicity experiments to demonstrate whether there is potential toxicity of ABO to the mice. We evaluated the influence of ABO on the weight of body and various organs, that is, heart, liver, spleen, lungs, kidney and brain, and so on, and the organ coefficients were calculated (Figure 8a and Supplementary Table S1). The results showed that there were no significant differences in body weight and organ coefficients between the control group and ABO-treated groups.

Furthermore, ABO treatment did not affect plasma lipid levels in mice (Figure 8b). Therefore, the anti-atherogenic effect of ABO was not related to lipid metabolism in apoE $^{-/-}$ mice.

Inhibition of PC-PLC by ABO suppressed oxLDL-induced IL-6 and IL-8 secretion in HUVECs. As our recent *in vivo* study demonstrated that PC-PLC contributed to the progression of atherosclerosis by promoting the production of pro-inflammatory cytokines, the secretions of inflammation related factors, such IL-6 and IL-8, from cultured HUVECs were measured by enzyme-linked immunosorbent assay. The results showed that treatment of HUVECs with ABO blunted the increase of IL-6 and IL-8 secretion induced by oxLDL (Figure 8c).

Discussion

Atherosclerosis and its complications are becoming the leading cause of death among the elderly.[28] Currently, surgery or drug treatments were the common therapeutic options available for patients with atherosclerosis, both of which have their drawbacks. Surgical treatment may be impossible or dangerous in patients with advance atherosclerosis and the complication rate is relatively high. The conventional drug treatment has side effects, and there remains a large unmet medical need in the treatment of advance atherosclerosis. Therefore, there is a clear need for development of new and more effective therapies for controlling advanced atherosclerosis, and existing agents, or novel compounds that target known key factors, may eventually be shown to have efficacy for treating and stabilizing advanced atherosclerosis. As endothelial injury represents a primary mechanism for acute clinical events by
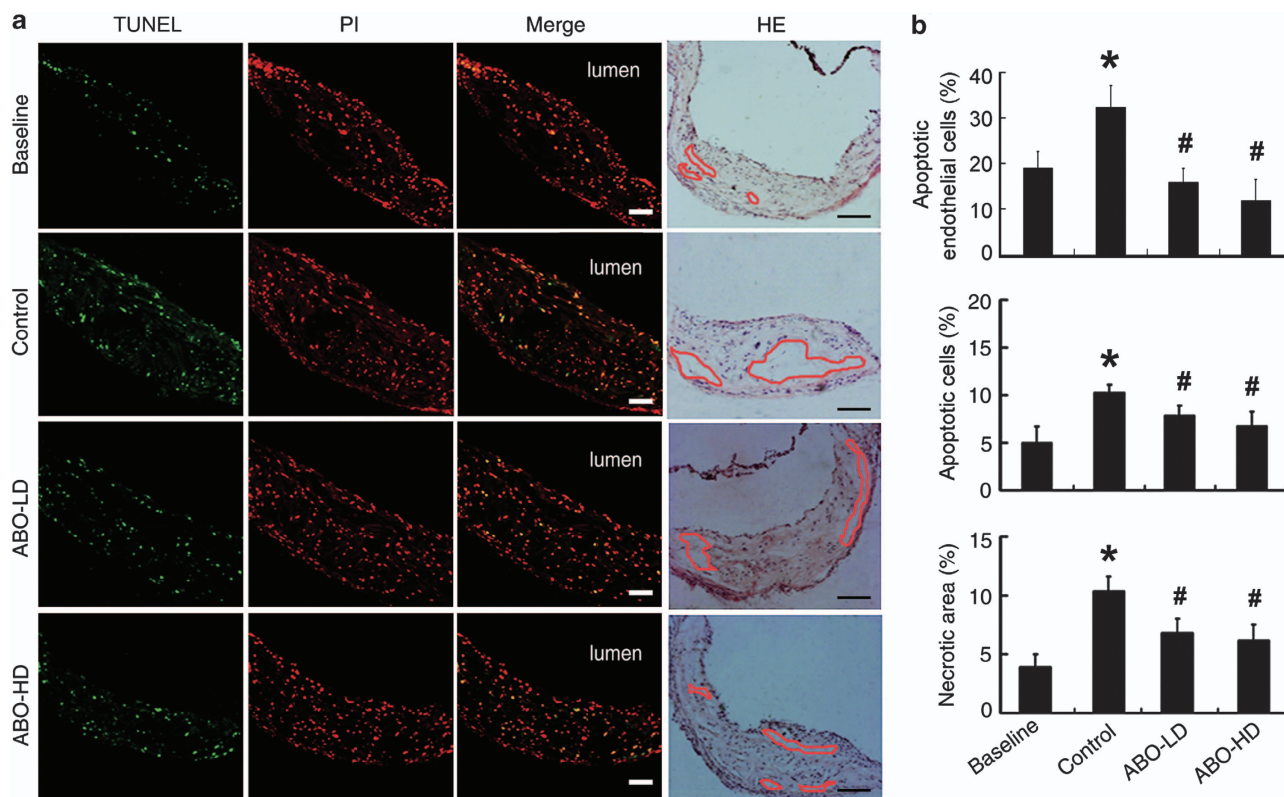
Figure 6 Images and quantifications of cell death in the aortic root lesions of apoE$^{-/-}$ mice. (**a**) Left, sections from the aortic root were labeled by TUNEL to detect apoptotic cells and counterstained with PI to detect nuclei; right, images of H&E-stained aortic root lesions. Red lines show the boundary of the developing necrotic core. Scale bars, 60 μm. (**b**) From the top to bottom panel, mean percent of TUNEL-positive cells in the lesions, TUNEL-positive cells in the endothelium and necrotic areas in the lesions. Values are mean ± S.E.M. *$P < 0.05$ versus baseline, #$P < 0.05$ versus control, $n = 6$

promoting lesion thrombosis, VECs have a significant impact on the stability of atherosclerotic plaques.[29] Our previous research demonstrated that ABO could avert VEC apoptosis induced by nutrient deprivation[30] and inhibit VEC apoptosis elicited by oxLDL,[10] which has been assumed as a major cause of endothelial dysfunction associated with proatherogenic conditions.[31] These findings suggested ABO as a protector of VECs. In this study, we further confirmed the beneficial effect of ABO on protecting VECs and inhibiting atherosclerosis progression in vivo.

As a phospholipid binding proteins, ANXA7 participates in phospholipid vesicles fusion and secretion cascade. Furthermore, ANX7 is a newly described candidate tumor suppressor gene for prostate cancer, as evidenced by a significantly higher rate of loss of ANX7 expression in metastatic and local recurrences of hormone refractory prostate cancer as compared with primary tumors.[14] ANXA7 exhibits many biological and genetic properties of a tumor suppressor gene and may have a role in carcinogenesis through a discrete signaling pathway involving other tumor suppressor genes, DNA-repair genes and apoptosis-related genes.[14,15] Besides, ANXA7($^{+/-}$) mutation leads to insulin secretion disorder in mice.[17] These reports indicated that ANXA7 might be invovled in several diseases. In the current study, we identified the anti-atherosclerotic role of ANXA7 for the first time, and compared with genetic modulation, ABO may be a powerful and ideal regulator of ANXA7 for atherosclerosis treatment.

A recent in vitro study demonstrated that pharmacological induction of autophagy in macrophages triggered secretion of pro-inflammatory cytokines,[32] which suggests that the pro-inflammatory effects of drug-induced autophagy should not be neglected when designing pharmacological interventions aimed at stabilizing atherosclerotic plaques via autophagy. We found that ABO could significantly decrease the secretion of IL-6 and IL-8, and the level and activity of PC-PLC, a major pro-inflammatory factor in atherosclerosis, accompanying enhanced autophagy in VECs. A recent study reported that stimulation of autophagy could only be beneficial if autophagic flux was not impaired, because this condition could lead to lysosomal leakage or ejection of autophagosomes, as well as cell death.[33] Until now, we lacked data on autophagic flux during atherosclerotic plaque formation and destabilization. Our use of TEM revealed autophagic vacuoles, including double- or single-membrane vesicles with intracellular contents (cytosol and organelles), namely autophagosomes and autolysosomes, in VECs of ABO-treated apoE$^{-/-}$ mice. According to a recent report,[34] our TEM morphological data may suggest in part that autophagic flux is increased in ABO-treated apoE$^{-/-}$ mice endothelium. To confirm the autophagic activation in VECs, we performed en face immufluorescence analysis of LC3 puncta, whose changes could reflect in vivo autophagy status.[21] Consistently, the punctate LC3 was significantly increased by ABO treatment. Thus, autophagic flux in the atherosclerotic endothelium was increased by
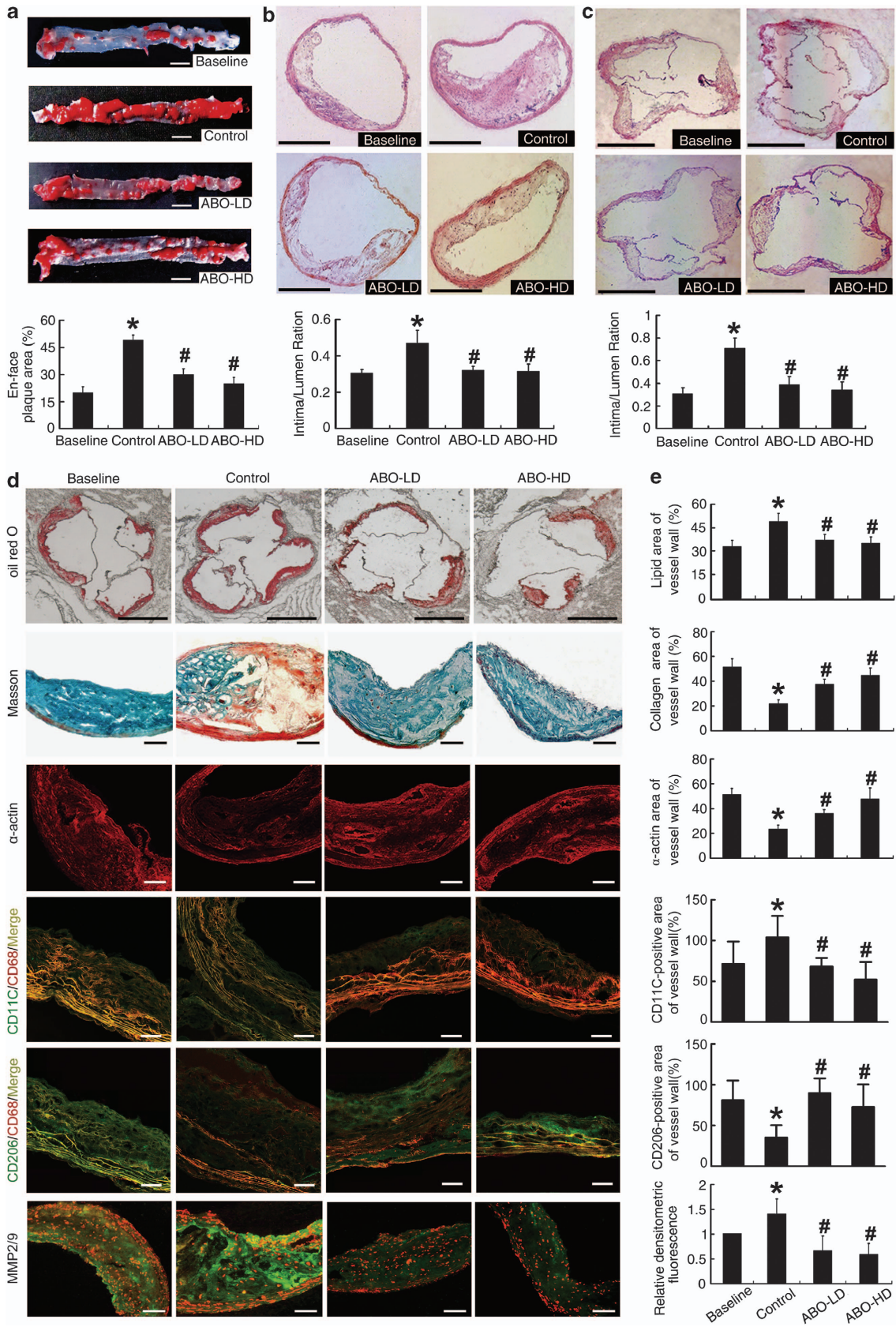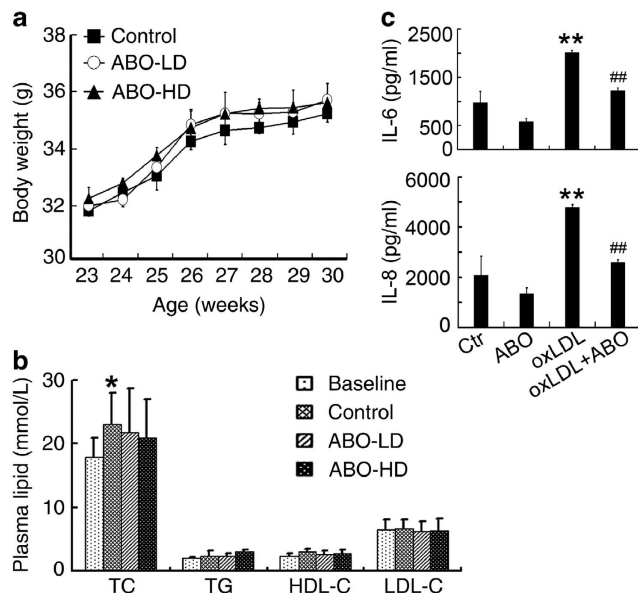
ABO treatment. We revealed the protective anti-atherosclerotic properties and possible mechanisms of autophagy induced by ABO in VECs of atherosclerotic plaques without activating unwanted pro-inflammatory signaling cascades.

Recent[8] and current studies by our group showed that PC-PLC may be an attractive target for anti-atherosclerosis therapy. Several inhibitors of PC-PLC have been identified, with D609 having a prominent place. A series of 2-aminohydroxamic acid derivatives have been designed as inhibitors of *Bacillus cereus* phospholipase C (PC-PLCBc), which has antigenic similarity with mammalian PC-PLC.[35] Chinese propolis has an anti-inflammatory effect in part by its inhibitory effect on the activity of PC-PLC.[36] Our data highlight ABO as a small molecular inhibitor of PC-PLC for the first time and identify ANXA7 as an unprecedented endogenous regulator of PC-PLC.

In summary, our data highlight the role of ANXA7 in the negative regulation of PC-PLC activity in VECs, and ANXA7/PC-PLC signaling pathway may represent a novel target for the treatment of atherosclerosis.

Materials and Methods

Cell culture. HUVECs were obtained from human umbilical cord veins as described.[37] MS1 cells were obtained from the Cell Bank of the Chinese Academy of Sciences (Shanghai, China). All lines were maintained at 37 °C under humidified conditions and 5% CO_2. HUVECs were cultured as routine on gelatin-coated plastic dishes in M199 medium (Gibco Laboratories, Grand Island, NY, USA) supplemented with 10% heat-inactivated fetal bovine serum (HyClone Laboratories, Logan, UT, USA) and 70 ng/ml basic fibroblast growth factor. All experiments involved HUVECs at passages 10–20. MS1 cells were cultured as routine in DMEM medium (Gibco Laboratories) supplemented with 10% heat-inactivated fetal bovine serum.

Antibodies. Antibodies for CD11C/Integrin αX (sc-28671), CD206 (sc-58987), CD68 (sc-7084), α-actin (sc-32251), CD31/PECAM-1 (sc-18916), ANXA7 (sc-11389), β-actin (sc-47778), GAPDH (sc-365062) and horseradish peroxidase-conjugated secondary antibodies were obtained from Santa Cruz Biotechnology (Santa Cruz, CA, USA). Antibodies against p62 (610833) and (PM045) were obtained from BD Transduction Laboratories (San Jose, CA, USA) and MBL International (Woburn, MA, USA), respectively. Antibody for LC3B (2775) was obtained from Cell Signaling Technology (Danvers, MA, USA). Normal rabbit IgG (sc-2027, Santa Cruz Biotechnology) was a control for immunofluorescence assay. Rabbit polyclonal antibody against PC-PLC was raised against *B. cereus* phospholipase C (PC-PLCBc), which has selective cross-reactivity against mammalian PC-PLC.[38] Secondary antibodies for immunofluorescence were goat anti-rabbit IgG Alexa Fluor-488, anti-rat IgG Alexa Fluor-633, goat anti-rat Alexa 488, donkey anti-goat Alexa 633 and donkey anti-rabbit Alexa 546 (Invitrogen, Carlsbad, CA, USA).

Western blot analysis. Protein samples (20 μg/lane) were loaded on a 15% SDS-polyacrylamide gel, separated and electrophoretically transferred to a polyvinylidene difluoride membrane (Millipore, Schwalbach, Germany), which was probed with primary antibodies, then horseradish peroxidase-linked secondary antibodies and revealed with use of an enhanced chemiluminesence detection kit (Thermo Electron Corp., Rockford, IL, USA). The relative quantity of proteins was analyzed by use of Quantity one software and normalized to that of loading controls.

Overexpression of ANXA7. HUVECs were obtained from human umbilical cord veins as described.[37] Cells were transfected by the TurboFectin 8.0 reagent method (TF81001, Origene, Rockville, MD, USA). We used pcmv 6-xl5-ANXA7 (SC126802, Origene) for ANXA7 overexpression, with pcmv 6-xl5 as a control. Transfection efficiency was examined by western blot analysis and immunofluorescence.

RNA interference. ANXA7 silencing in HUVECs was as described[11] with specific ANXA7. In total, 40 nM ANXA7 siRNA were transfected into HUVECs by the use of RNAiFect Transfection Reagent (301605, Qiagen, Hilden, Germany). Scrambled siRNA was used as a control (1022076, Qiagen). Silencing efficiency was verified by western blot analysis or immunofluorescence.

Cell staining for immunofluorescence microscopy. HUVECs were fixed in 4% paraformaldehyde (w/v) for 30 min at room temperature and blocked in 1 × phosphate-buffered saline (PBS), 0.01% Triton X-100 (v/v) and 5% goat serum (v/v), and then incubated with primary antibodies overnight at 4 °C. Then cells were rinsed in 1 × PBS three times and incubated with corresponding secondary antibodies 1 h at 37 °C. For negative controls, cells were incubated with normal IgG. CLSM involved a Leica TCS SP2 AOBS apparatus. Different fields of view (>3 regions) were analyzed on the microscope for each labeling condition, and representative results are shown.

Figure 8 Effects of ABO on body weight, organ coefficients and serum lipid levels of apoE$^{-/-}$ mice and oxLDL-induced IL-6 and IL-8 secretion in HUVECs. (**a**) Body weight was measured every week. Data are mean ± S.E.M.; $n = 6$. (**b**) Blood was collected at the end of the experiment for measuring lipid levels. Data are mean ± S.E.M. *$P < 0.05$ *versus* baseline, $n = 6$. (**c**) ABO decreased the secretion of IL-6 and IL-8 from oxLDL-treated HUVECs. ABO (50 μM) and oxLDL (50 μg/ml) were used. IL-6 and IL-8 secretions from HUVECs were measured by enzyme-linked immunosorbent assay. Data are mean ± S.E.M. **$P < 0.01$ *versus* control, ##$P < 0.01$ *versus* oxLDL, $n = 3$

Figure 7 Effects of ABO on the size and phenotype of aortic atherosclerotic plaque in apoE$^{-/-}$ mice. (**a**) Representative oil-red O–stained aortas from apoE$^{-/-}$ mice (Scale bars, 3 mm, $n = 5$). (**b**) H&E staining of brachiocephalic artery (scale bars, 200 μm, $n = 6$) and (**c**) aortic root lesions (scale bars, 500 μm, $n = 6$). Bar graphs show en face plaque area and ratio of intima to lumen (data are mean ± S.E.M. *$P < 0.05$ *versus* baseline, #$P < 0.05$ *versus* control). (**d**) From the top to bottom panel, oil-red O staining of atherosclerotic lesions, masson trichrome staining of collagen (in blue), immunostaining for mouse α-smooth muscle actin, double-stained images of co-localization (yellow) of CD68 (red) and CD11C (green)-positive areas, double-stained images of co-localization (yellow) of CD68 (red) and CD206 (green) -positive areas and *in situ* zymography detecting MMP-2/9 activity ($n = 4$–5 sections per tissue, at least three sites of analysis per slide). Scale bars for oil-red O staining, 500 μm and others, 80 μm. (**e**) Quantification of lipid, collagen, actin area in atherosclerotic lesion, weighted co-localization coefficients for CD11C and CD206-positive areas, and MMP-2/9 activity in baseline, control and ABO-treated groups. Data are mean ± S.E.M. *$P < 0.05$ *versus* baseline, #$P < 0.05$ *versus* control, $n = 6$

PC-PLC activity assay. PC-PLC activity was measured by the Amplex Red PC-PLC-specific assay kit (Molecular Probes A12218, Eugene, OR, USA) with modification.[39] After several steps of enzyme-coupled reactions with 10-acetyl-3, 7-dihydrophenoxazine (Amplex Red reagent), alkaline phosphatase, choline oxidase and horseradish peroxidase, PC-PLC in whole-cell lysates and serum converted PC (egg yolk lecithin) substrate to highly fluorescent product resorufin.

Animals. Male apoE$^{-/-}$ mice (8 weeks old, 20–25 g; B6.129P2-Apoetm1Unc/J, stock no. 002052) on a C57BL/6J background were purchased from the Department of Laboratory Animal Science, Peking University Health Science Center (Beijing, China), and housed under pathogen-free conditions. The experimental design of the study was shown in Supplementary Figure S5, and all mouse work was performed according to the Institutional Animal Care and Use Committee guidelines. Mice were fed with an atherogenic high-fat diet (21% fat and 0.15% cholesterol) for 14 weeks. Body weight was measured during treatment and plasma lipid profiles at baseline, and at the end of the experiment. Animals were randomized to four groups ($n = 6$ mice/group) for treatment. The first group was killed to determine the extent of established lesions. Groups 2 and 3 received 8 weekly intraperitoneal injections of ABO (low-dosage, 50 mg/kg per day or high-dosage, 100 mg/kg per day). Control group 4 was injected with the same volume (10 μl) of dimethyl sulfoxide (Sigma-Aldrich, St. Louis, MO, USA) diluted with 90 μl PBS. At the end of treatment, all mice were killed by intravenous injection of ketamine/xylazine (Sigma-Aldrich), and blood and tissue were collected for analysis. The experimental protocol was approved by the local animal research committee.

Body-weight measurement and blood and tissue collection. Body weight in mice was measured during treatment and plasma lipid profiles at the end of the experiment. For mice at 22 and 30 week of age, food was removed for an 8-h fast, then blood was collected from the inferior vena cava, and animals were killed by exsanguination. The heart and aorta were rapidly removed after perfusion with PBS. The adventitia was thoroughly stripped, and the heart, including the aortic root, was snap-frozen in optimal cutting temperature embedding medium (Tissue-Tek, Torrance, CA) for histology and immunofluorescence assay. The remaining aorta was opened longitudinally and fixed with 10% buffered formalin for measurement of the surface area covered by lipid-staining lesions. Brachiocephalic arteries were removed for further analysis.

Histology and immunofluorescence. The aortic root and brachiocephalic artery of mice were embedded in optimal cutting temperature. Cryosections of aortic sinus (7 μm) and brachiocephalic artery (10 μm) were prepared and stained with hematoxylin (Sigma-Aldrich, Zwijndrecht, The Netherlands) and eosin (Merck, Darmstadt, Germany). Aortic root cryosections, 10 μm, underwent Oil-red O and Masson's trichrome staining (Maixin_Bio, Fuzhou, China). Images of sections were taken with a digital camera and analyzed by use of ImagePro Plus. Corresponding sections (7 μm) were stained with primary antibodies and appropriate secondary antibodies as described. The negative control was nonimmune IgGs (Supplementary Figure S6). Sections were observed by confocal laser scanning microscopy (CLSM, TCS SP2, Leica, Bensheim, Germany).

Transmission electron microscopy. TEM was performed as previously described.[40] 10 ultrathin sections per mouse were examined and photographed by use of a JOEL 1200EX electron microscope (JEOL, Tokyo, Japan). About 30 cells per mouse were assessed in this study.

En face aortic arch immunofluorescence. After perfusion fixation and dissection, the ascending aorta and proximal arch segment were incubated with 20% horse serum for 30 min. Each aortic arch was then incubated simultaneously with rat-anti-CD31 and rabbit-anti-LC3, followed by the appropriate combination of secondary antibodies: goat anti-rat Alexa 488 and donkey anti-rabbit Alexa 546 (Invitrogen). The nuclei were stained with DAPI and slides mounted in SlowFade Gold (Invitrogen). For negative controls, segments were incubated with normal IgG. Fluorescence images were obtained using the Zeiss LSM780 (Carl Zeiss Canada Ltd). Carl Zeiss ZEN 2010 Program was used to measure the fluorescence intensity, which was measured in at least 10 regions for each labeling condition, and representative results were shown.

Cell death in atherosclerotic plaque. Apoptotic cells in atherosclerotic lesions were detected by terminal deoxynucleotidyl transferase-mediated dUTP nick-end labeling (TUNEL, Promega, Madison, WI).[41,42] Plaque necrosis was quantified by measuring negative H&E-stained acellular areas in the intima.[43,44]

En Face staining. En face staining of plaque area in mice was measured as described. Briefly, after tissues were trimmed from around the aorta, including all fat, the aorta was opened longitudinally, pinned on a cork board, and stained with Oil-red O (Sigma-Aldrich to detect lipids and to determine lesion area. En face images of the aorta were taken with a digital camera (Nikon D7000, Nikon Corp., Tokyo, Japan) and analyzed by use of ImagePro Plus. Atherosclerotic lesions of the aorta were expressed as a percentage of the total surface area.

***In situ* zymography.** Aortic sections (7 μm) of mice were incubated with 50 μl of 10 μg/ml quenched FITC-labeled DQ gelatin (Invitrogen) and 1 μg/ml propidium iodide (PI, Sigma-Aldrich, St. Louis, MO) in 0.5% low melting point agarose (Invitrogen), cover-slipped, and chilled for 5 min at 4 °C. Sections were incubated at 37 °C for 2 h and observed by fluorescence microscopy. Gelatinase inhibitor (MMP-2/9 inhibitor IV, Chemicon, Millipore) was added as a control. Carl Zeiss AxioVision 4.6 was used to measure fluorescence intensity in at least six sections from each aortic root sample.

Organ coefficients. When mice were killed, various organs such as heart, liver, spleen, lungs, kidney and brain were removed and weighed. The organ coefficient was obtained by dividing the weight of the organ by body weight.

Serum lipid levels. The concentrations of total cholesterol, triglycerides, high-density lipoprotein cholesterol and low-density lipoprotein cholesterol in mice were determined enzymatically with available kits (Wako Chemicals USA, Richmond, VA, USA). All assays were completed in triplicate and all samples were analyzed on the same day.

Enzyme-linked immunosorbent assay (ELISA). The amount of IL-6 or IL-8 secreted into the culture medium was determined by ELISA using the human IL-6 or IL-8 kit (R&D Systems, Minneapolis, MN, USA), respectively. These assays were performed according to the manufacturer's instructions, and the data were expressed relative to a standard curve prepared for IL-6 or IL-8.

Statistical analyses. Data are expressed as mean ± S.E.M. SPSS 11.5 (SPSS Inc., Chicago, IL, USA) was used for statistical analysis. Data were analyzed by one-way ANOVA (followed by Scheffé F-test for *post hoc* analysis). $P < 0.05$ was considered statistically significant.

Conflict of Interest

The authors declare no conflict of interest.

1. Rikiishi H. Novel insights into the interplay between apoptosis and autophagy. *Int J Cell Biol* 2012; **2012**: 317645.
2. Kang R, Zeh HJ, Lotze MT, Tang D. The Beclin 1 network regulates autophagy and apoptosis. *Cell Death Differ* 2011; **18**: 571–580.
3. Szumilo M, Rahden-Staron I. [Biological role of phosphatidylcholine-specific phospholipase C in mammalian cells]. *Postepy Hig Med Dosw (Online)* 2008; **62**: 593–598.
4. Li H, Zhang L, Yin D, Zhang Y, Miao J. Targeting phosphatidylcholine-specific phospholipase C for atherogenesis therapy. *Trends Cardiovasc Med* 2010; **20**: 172–176.
5. Miao JY, Kaji K, Hayashi H, Araki S. Suppression of apoptosis by inhibition of phosphatidylcholine-specific phospholipase C in vascular endothelial cells. *Endothelium* 1997; **5**: 231–239.
6. Dong Z, Wang L, Xu J, Li Y, Zhang Y, Zhang S et al. Promotion of autophagy and inhibition of apoptosis by low concentrations of cadmium in vascular endothelial cells. *Toxicol In Vitro* 2009; **23**: 105–110.

7. Ge D, Jing Q, Meng N, Su L, Zhang Y, Zhang S et al. Regulation of apoptosis and autophagy by sphingosylphosphorylcholine in vascular endothelial cells. J Cell Physiol 2011; 226: 2827–2833.

8. Zhang L, Zhao J, Su L, Huang B, Wang L, Su H et al. D609 inhibits progression of preexisting atheroma and promotes lesion stability in apolipoprotein e-/- mice: a role of phosphatidylcholine-specific phospholipase in atherosclerosis. Arterioscler, Thromb Vasc Biol 2010; 30: 411–418.

9. Liu H, Zhang H, Forman HJ. Silica induces macrophage cytokines through phosphatidylcholine-specific phospholipase C with hydrogen peroxide. Am J Respir Cell Mol Biol 2007; 36: 594–599.

10. Liu X, Zhao J, Xu J, Zhao B, Zhang Y, Zhang S et al. Protective effects of a benzoxazine derivative against oxidized LDL-induced apoptosis and the increases of integrin beta4, ROS, NF-kappaB and P53 in human umbilical vein endothelial cells. Bioorg Med Chem Lett 2009; 19: 2896–2900.

11. Wang L, Dong Z, Huang B, Zhao B, Wang H, Zhao J et al. Distinct patterns of autophagy evoked by two benzoxazine derivatives in vascular endothelial cells. Autophagy 2010; 6: 1115–1124.

12. Caohuy H, Pollard HB. Activation of annexin 7 by protein kinase C in vitro and in vivo. J Biol Chem 2001; 276: 12813–12821.

13. Park MJ, Park IC, Hur JH, Rhee CH, Choe TB, Yi DH et al. Protein kinase C activation by phorbol ester increases in vitro invasion through regulation of matrix metalloproteinases/tissue inhibitors of metalloproteinases system in D54 human glioblastoma cells. Neurosci Lett 2000; 290: 201–204.

14. Srivastava M, Bubendorf L, Srikantan V, Fossom L, Nolan L, Glasman M et al. ANX7, a candidate tumor suppressor gene for prostate cancer. Proc Natl Acad Sci USA 2001; 98: 4575–4580.

15. Srivastava M, Montagna C, Leighton X, Glasman M, Naga S, Eidelman O et al. Haploinsufficiency of Anx7 tumor suppressor gene and consequent genomic instability promotes tumorigenesis in the Anx7($+/-$) mouse. Proc Natl Acad Sci USA 2003; 100: 14287–14292.

16. Herr C, Smyth N, Ullrich S, Yun F, Sasse P, Hescheler J et al. Loss of annexin A7 leads to alterations in frequency-induced shortening of isolated murine cardiomyocytes. Mol Cell Biol 2001; 21: 4119–4128.

17. Mears D, Zimliki CL, Atwater I, Rojas E, Glassman M, Leighton X et al. The Anx7($+/-$) knockout mutation alters electrical and secretory responses to Ca(2+)-mobilizing agents in pancreatic beta-cells. Cell Physiol Biochem 2012; 29: 697–704.

18. Li H, Liu N, Wang S, Wang L, Zhao J, Su L et al. Identification of a small molecule targeting annexin A7. Biochim Biophys Acta 2013; 1832: 2092–2099.

19. Caohuy H, Pollard HB. Protein kinase C and guanosine triphosphate combine to potentiate calcium-dependent membrane fusion driven by annexin 7. J Biol Chem 2002; 277: 25217–25225.

20. Chander A, Chen XL, Naidu DG. A role for diacylglycerol in annexin A7-mediated fusion of lung lamellar bodies. Biochim Biophys Acta 2007; 1771: 1308–1318.

21. Barth S, Glick D, Macleod KF. Autophagy: assays and artifacts. J Pathol 2010; 221: 117–124.

22. Bjorkoy G, Lamark T, Pankiv S, Overvatn A, Brech A, Johansen T. Monitoring autophagic degradation of p62/SQSTM1. Methods Enzymol 2009; 452: 181–197.

23. Liao X, Sluimer JC, Wang Y, Subramanian M, Brown K, Pattison JS et al. Macrophage autophagy plays a protective role in advanced atherosclerosis. Cell Metab 2012; 15: 545–553.

24. Razani B, Feng C, Coleman T, Emanuel R, Wen H, Hwang S et al. Autophagy links inflammasomes to atherosclerotic progression. Cell Metab 2012; 15: 534–544.

25. Kolodgie FD, Petrov A, Virmani R, Narula N, Verjans JW, Weber DK et al. Targeting of apoptotic macrophages and experimental atheroma with radiolabeled annexin V: a technique with potential for noninvasive imaging of vulnerable plaque. Circulation 2003; 108: 3134–3139.

26. Schwartz SM, Galis ZS, Rosenfeld ME, Falk E. Plaque rupture in humans and mice. Arterioscler Thromb Vasc Biol 2007; 27: 705–713.

27. Hirata Y, Tabata M, Kurobe H, Motoki T, Akaike M, Nishio C et al. Coronary atherosclerosis is associated with macrophage polarization in epicardial adipose tissue. J Am Coll Cardio 2011; 58: 248–255.

28. Glass CK, Witztum JL. Atherosclerosis. the road ahead. Cell 2001; 104: 503–516.

29. Martinet W, De Meyer GR. Autophagy in atherosclerosis. Curr Atheroscler Rep 2008; 10: 216–223.

30. Jiao PF, Zhao BX, Wang WW, He QX, Wan MS, Shin DS et al. Design, synthesis, and preliminary biological evaluation of 2,3-dihydro-3-hydroxymethyl-1,4-benzoxazine derivatives. Bioorg Med Chem Lett 2006; 16: 2862–2867.

31. Ross R. Cell biology of atherosclerosis. Annl Rev Physiol 1995; 57: 791–804.

32. Schrijvers DM, De Meyer GR, Martinet W. Autophagy in atherosclerosis: a potential drug target for plaque stabilization. Arterioscler Thromb Vasc Biol 2011; 31: 2787–2791.

33. Gottlieb RA, Mentzer RM. Autophagy during cardiac stress: joys and frustrations of autophagy. Ann Rev Physiol 2010; 72: 45–59.

34. Zheng Q, Su H, Ranek MJ, Wang X. Autophagy and p62 in cardiac proteinopathy. Circ Res 2011; 109: 296–308.

35. Gonzalez-Bulnes P, Gonzalez-Roura A, Canals D, Delgado A, Casas J, Llebaria A. 2-aminohydroxamic acid derivatives as inhibitors of Bacillus cereus phosphatidylcholine preferred phospholipase C PC-PLC(Bc). Bioorg Med Chem 2010; 18: 8549–8555.

36. Xuan H, Zhu R, Li Y, Hu F. Inhibitory effect of chinese propolis on phosphatidylcholine-specific phospholipase C activity in vascular endothelial cells. Evid Based Complement Alternat Med 2011; 2011: 985278.

37. Jaffe EA, Nachman RL, Becker CG, Minick CR. Culture of human endothelial cells derived from umbilical veins. Identification by morphologic and immunologic criteria. J Clin Invest 1973; 52: 2745–2756.

38. Spadaro F, Ramoni C, Mezzanzanica D, Miotti S, Alberti P, Cecchetti S et al. Phosphatidylcholine-specific phospholipase C activation in epithelial ovarian cancer cells. Cancer Res 2008; 68: 6541–6549.

39. Spadaro F, Cecchetti S, Sanchez M, Ausiello CM, Podo F, Ramoni C. Expression and role of phosphatidylcholine-specific phospholipase C in human NK and T lymphocyte subsets. Eur J Immunol 2006; 36: 3277–3287.

40. Wang X, Osinska H, Klevitsky R, Gerdes AM, Nieman M, Lorenz J et al. Expression of R120G-alphaB-crystallin causes aberrant desmin and alphaB-crystallin aggregation and cardiomyopathy in mice. Circ Res 2001; 89: 84–91.

41. Hein S, Arnon E, Kostin S, Schonburg M, Elsasser A, Polyakova V et al. Progression from compensated hypertrophy to failure in the pressure-overloaded human heart: structural deterioration and compensatory mechanisms. Circulation 2003; 107: 984–991.

42. Elsasser A, Vogt AM, Nef H, Kostin S, Mollmann H, Skwara W et al. Human hibernating myocardium is jeopardized by apoptotic and autophagic cell death. J Am Coll Cardiol 2004; 43: 2191–2199.

43. Feng B, Zhang D, Kuriakose G, Devlin CM, Kockx M, Tabas I. Niemann-Pick C heterozygosity confers resistance to lesional necrosis and macrophage apoptosis in murine atherosclerosis. Proc Natl Acad Sci USA 2003; 100: 10423–10428.

44. Thorp E, Li Y, Bao L, Yao PM, Kuriakose G, Rong J et al. Brief report: increased apoptosis in advanced atherosclerotic lesions of Apoe-/- mice lacking macrophage Bcl-2. Arterioscler Thromb Vasc Biol 2009; 29: 169–172.